Journal of Computational and Applied Mathematics 289 (2015) 306–321

Contents lists available at ScienceDirect

Journal of Computational and Applied Mathematics

journal homepage: www.elsevier.com/locate/cam

Local multiple traces formulation for high-frequency scattering problems☆

Carlos Jerez-Hanckes *, José Pinto, Simon Tournier

School of Engineering, Pontificia Universidad Católica de Chile, Av. Vicuña Mackenna 4860, Macul, Santiago, Chile

ARTICLE INFO

Article history:
Received 18 September 2014
Received in revised form 30 November 2014

Keywords:
Boundary integral equations
Spectral elements
Multiple traces formulation
Preconditioning
High-frequency scattering

ABSTRACT

We present an efficient method to solve high-frequency scattering problems by heterogeneous penetrable objects in two dimensions. This is achieved by extending the so-called *Local Multiple Traces Formulation*, introduced recently by Hiptmair and Jerez-Hanckes, to purely spectral discretizations employing weighted Chebyshev polynomials. Together with regularization strategies to handle boundary integral operators singularities, matrix entries are quickly computed via the Fast Fourier Transform. The resulting Fredholm first-kind formulation is free from spurious resonances, and though ill-conditioned, it possesses built-in Calderón-type preconditioners. Numerical results obtained for different settings validate our claims and greatly motivate future research in this direction.

1. Introduction

Many areas in engineering ranging from biomedical imaging via ultrasound or electromagnetic waves to the design of antennae and telescopes, greatly profit from the ever-increasing computational processing capacity to simulate wave scattering. After decades of development, Boundary Integral (BI)-based techniques [1], also known as the Method of Moments (MoM), have rightfully gained their place among the modeling tools available for mathematicians, physicists and engineers. By employing the appropriate Green's functions, these methods portray wave propagation in the entire unbounded homogeneous space by solving first or second kind Fredholm boundary integral equations (BIEs) on the surface of the scatterers. However, in most realistic scenarios, e.g., whenever scatterers are composed of several distinct parts of largely different sizes, standard discretization of the BIEs leads to large dense linear systems for which existing iterative solving algorithms perform poorly. Indeed, a fixed number of degrees of freedom is mandatory per wavelength in order to represent oscillatory solutions quickly leading to prohibitive computational expenses. Moreover, the conditioning number of the matrices obtained can be shown to increase with the wavenumber.

Several solution strategies have been proposed to deal with this so-called *high frequency* problem. One approach seeks to find faster implementations of standard methods, such as fast multipole methods [2–5]. Another body of work relies on asymptotic techniques such as geometrical optics, physical optics and the geometrical theory of diffraction [6,7]. Such approximations are computationally cheap but generally accurate only for sufficiently high frequencies. Hence, questions arise as to when and how these techniques should be applied and what to do in situations that require accommodating different ranges of frequencies as in the case of highly contrasting materials (heterogeneous scatters). Taking a different direction, and perhaps closer to our work, Bruno and co-workers [8,9] have solved the arising high-frequency BIEs using spectral techniques for Nyström methods for perfectly conducting scatterers.

☆ This research was partially funded by FONDECYT Iniciación 11121166 and CONICYT Anillo ACT1118 (ANANUM).
* Corresponding author.
E-mail addresses: cjerez@ing.puc.cl (C. Jerez-Hanckes), jspinto@uc.cl (J. Pinto), simon.tournier@alumni.enseeiht.fr (S. Tournier).

http://dx.doi.org/10.1016/j.cam.2014.12.045
0377-0427/

As it usually happens, algorithm hybridization may bring the best of worlds. More precisely, one seeks to incorporate asymptotic information of the highly oscillatory nature of the problem into the approximation space, yielding *Hybrid Numerical-Asymptotic* (HNA) methods [10–15]. Although most of these efforts focus on impenetrable scatterers, Groth et al. [16] have recently proposed an adaptation of the HNA approach to deal with a single penetrable object but the extension to heterogeneous scatterers is unclear.

Hence, the question remains: is it possible to solve scattering problems for heterogeneous objects portraying a large frequency range in practical terms? To answer this, we will follow the spirit of the *Multiple Traces Formulations* (MTFs) [17–20] and tackle two-dimensional composite scatterers with largely varying wavenumbers. In particular, we will focus on a variant dubbed *local* since all unknown boundary traces and test functions are locally defined on subdomain boundaries. As a Galerkin–Petrov formulation, transmission conditions are enforced weakly by testing with also locally defined test functions. On the continuous level, the resulting first-kind Fredholm equation possesses unique solutions. Hence, the formulation is more robust than other formulations, as it naturally rejects spurious resonances, i.e. non-trivial but unphysical solutions for certain exterior wavenumbers. Moreover, the resulting block diagonal structure hints at its amenability to parallelization and operator preconditioning. Numerical analysis and results in two and three dimensions already validated this for low-order elements. However, and as expected, such discretization bases are not sufficient for high-frequency regimes, and so we will explore a purely *spectral* or *p*-refinement approximation for boundary unknowns. In doing so, we will further extend the mathematical formalism provided for the local MTF to account for piecewise Cauchy data and show that the formulation lends itself to preconditioning quite easily.

Outline. In Section 2 we recall and generalize the derivation of local MTF for piecewise traces, which requires imposing Calderón identities weakly. Readers may skip technical Sections 2.1, 2.3 and 2.4 to check the final formulation in 2.5. Spectral discretization will be carried out using Chebyshev polynomials as shown in Section 3. There we present the numerical analysis required for deducing existence and uniqueness on the discrete level as well as bounds on the errors based on projection estimates over weighted Sobolev spaces. Moreover, we discuss the efficient implementation using fast Fourier techniques (FFT). Numerical results portraying the efficiency and power of the method proposed are introduced in Section 4 for the simple setting of a circle divided in two halves. This configuration already presents the difficulties inherent to the problem: triple points and different wavenumbers. Particular attention is given to error convergence and to the effect of diagonal preconditioning on iterative solvers as shown in Section 4.5. Conclusions and future directions are drawn in Section 5.

2. Generalized local multiple traces formulation

2.1. Functional spaces

Let $\mathcal{O}$ be a bounded closed domain. We denote by $L^p(\mathcal{O})$, $\mathcal{D}(\mathcal{O})$, $\mathcal{D}'(\mathcal{O})$ and $H^s(\mathcal{O})$, the standard Lebesgue space for $p \in [1, \infty]$, the space of C^∞-compactly supported functions, the space of distributions, and Sobolev spaces for $s \geq 0$, respectively, all defined over $\mathcal{O}$ [21]. If $\mathcal{O}$ has a boundary, we assume that it can be extended to a closed manifold $\widetilde{\mathcal{O}}$, with $\mathcal{O} \subset \widetilde{\mathcal{O}}$, and write $\widetilde{u}$ for the extension of u by zero over $\widetilde{\mathcal{O}}$. For $s > 0$ and $\mathcal{O}$ Lipschitz, one defines the closed subspace of $\widetilde{H}^s(\mathcal{O})$:

$$\widetilde{H}^s(\mathcal{O}) := \{u \in H^s(\mathcal{O}) : u \in H^s(\widetilde{\mathcal{O}})\} \tag{1}$$

provided with the norm $\|u\|_{\widetilde{H}^s(\mathcal{O})} = \|\widetilde{u}\|_{H^s(\widetilde{\mathcal{O}})}$, where the last norm is the standard one. For $s < 0$ we use the L^2-duality product so that $\widetilde{H}^s(\mathcal{O})$ is the dual of $H^{-s}(\mathcal{O})$. We will be particularly interested in the following subspaces:

$$\widetilde{H}^{-1/2}(\mathcal{O}) = \left(H^{1/2}(\mathcal{O})\right)' \quad \text{and} \quad H^{1/2}(\mathcal{O}) = \left(\widetilde{H}^{1/2}(\mathcal{O})\right)'. \tag{2}$$

2.2. Model problem

Without loss of generality, we consider the geometric arrangement shown in Fig. 1 where $\Omega := \bar{\Omega}_1 \cup \bar{\Omega}_2$ is a heterogeneous simply connected scatterer, composed of two bounded simply connected subdomains $\Omega_1, \Omega_2 \in \mathbb{R}^2$. The exterior domain is denoted by $\Omega_0 := \mathbb{R}^2 \setminus \bar{\Omega}$ and interfaces by $\Gamma_{ij} := \partial\Omega_i \cap \partial\Omega_j$. We will make use of the index set $\Lambda_i = \{j \in \mathbb{N} : \partial\Omega_i \cap \partial\Omega_j \neq \emptyset\}$ for $i = 0, 1, 2$.

For an exciting plane wave u^{inc}, we seek u representing the field scattered in Ω_0 and total field in Ω which satisfy homogeneous Helmholtz equations, with constant wavenumbers $\kappa_i \in \mathbb{C} \setminus \mathbb{R}_-$ in each subdomain Ω_i, $i = 0, 1, 2$. Explicitly, we seek $u \in H^1_{\text{loc}}(\Omega \cup \Omega_0)$ such that

$$-\Delta u - \kappa_i^2 u = 0, \quad \forall \mathbf{x} \in \partial\Omega_i,\ i = 0, 1, 2, \tag{3a}$$

$$[\boldsymbol{\gamma} u] = \mathbf{g}, \quad \forall \mathbf{x} \in \Gamma_{01} \cup \Gamma_{02}, \tag{3b}$$

$$[\boldsymbol{\gamma} u] = \mathbf{0}, \quad \forall \mathbf{x} \in \Gamma_{12}, \tag{3c}$$

$$+ \text{radiation conditions} \quad \text{when } \|\mathbf{x}\| \to \infty. \tag{3d}$$

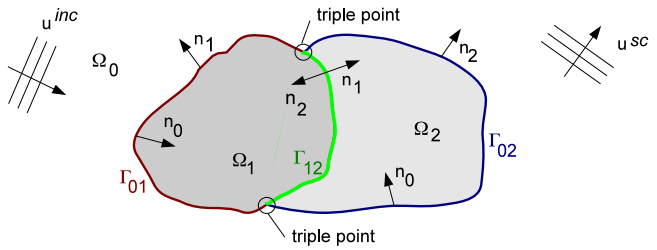

Fig. 1. Simple model geometry. Observe normal definitions.

Here we have used the notation $\boldsymbol{\gamma}^i := (\gamma_D^i, \gamma_N^i)$ for standard Dirichlet and Neumann interior traces on subdomain boundary $\partial\Omega_i$, so that (3b) and (3c) represent inhomogeneous, $\mathbf{g} = -\boldsymbol{\gamma} u^{\text{inc}} \in H^{1/2}(\partial\Omega_i)\times H^{-1/2}(\partial\Omega_i)$, and homogeneous transmission conditions, respectively, with $[\cdot]$ denoting trace jump across the indicated interface.

2.3. Weak transmission conditions

We now extend the local MTF to spectral elements as in [17]. Such elements will be defined per interface Γ_{ij}, so instead of working on standard functional spaces $\mathbf{V}_i := H^{1/2}(\partial\Omega_i) \times H^{-1/2}(\partial\Omega_i)$, we will rely on "broken" spaces:

$$\mathbf{V}_i^{\text{pw}} := H_{\text{pw}}^{1/2}(\partial\Omega_i) \times H_{\text{pw}}^{-1/2}(\partial\Omega_i), \qquad \widetilde{\mathbf{V}}_i := \widetilde{H}_{\text{pw}}^{1/2}(\partial\Omega_i) \times \widetilde{H}_{\text{pw}}^{-1/2}(\partial\Omega_i), \tag{4}$$

where

$$H_{\text{pw}}^{\pm 1/2}(\partial\Omega_i) := \{u \in \mathcal{D}'(\partial\Omega_i) : u|_{\Gamma_{ij}} \in H^{\pm 1/2}(\Gamma_{ij}),\ \forall j \in \Lambda_i\}, \tag{5}$$

and similarly for $\widetilde{H}_{\text{pw}}^{\pm 1/2}(\partial\Omega_i)$. Observe that $\mathbf{V}_i^{\text{pw}}$ and $\widetilde{\mathbf{V}}_i$ are dual to each other when taking the cross duality product between Cartesian elements $\langle\cdot,\cdot\rangle_\times$, e.g., $\langle \boldsymbol{\lambda}^i, \boldsymbol{\varphi}^j\rangle_\times := \langle \lambda_{\text{D}}^i, \boldsymbol{\varphi}_{\text{N}}^j\rangle + \langle \lambda_{\text{N}}^i, \varphi_{\text{D}}^j\rangle$.

Transmission conditions are weakly enforced across each interface Γ_{ij}. This is done via local restriction and normal orientation operators, such that adjacent normals are re-oriented. Then, extension by zero onto the adjacent subdomain boundary is required to set up a single subdomain boundary equation. For this, we make use of *restriction–orientation-and-extension operators*, $\widetilde{\mathsf{X}}_{ij}$ mapping $\mathbf{V}_j^{\text{pw}} \to \mathbf{V}_i^{\text{pw}}$ when defined in duality with $\widetilde{\mathbf{V}}_i$.

2.4. Weak Calderón identities

We define our unknowns on subdomains Ω_i as $\boldsymbol{\lambda}^i := (\lambda_D^i, \lambda_N^i) \in \mathbf{V}_i^{\text{pw}}$. Notice that these are not strictly Cauchy data. However, we can weakly enforce Calderón identities satisfied by each unknown locally. More specifically, integral representations in each subdomain are used to set up Calderón identities over boundaries $\partial\Omega_i$, such that for all $\boldsymbol{\varphi} \in \widetilde{\mathbf{V}}_i$ it holds

$$\begin{aligned}\langle \boldsymbol{\lambda}^i, \boldsymbol{\varphi}^i\rangle_\times &= \left\langle \left(\frac{1}{2}\mathrm{Id} + \mathsf{A}_i\right)\boldsymbol{\lambda}^i, \boldsymbol{\varphi}^i\right\rangle_\times \\ &= \left\langle \begin{pmatrix} \frac{1}{2}\mathrm{Id} - \mathsf{K}_i & \mathsf{V}_i \\ \mathsf{W}_i & \frac{1}{2}\mathrm{Id} + \mathsf{K}_i' \end{pmatrix} \begin{pmatrix} \lambda_{\text{D}}^i \\ \lambda_{\text{N}}^i \end{pmatrix}, \begin{pmatrix} \varphi_{\text{D}}^i \\ \varphi_{\text{N}}^i \end{pmatrix} \right\rangle_\times,\end{aligned}$$

where $\mathsf{A}_i : \mathbf{V}_i \to \mathbf{V}_i$ contains the standard weakly singular, double layer, adjoint double layer and hypersingular integral operators, denoted V_i, K_i, K_i' and W_i, respectively, over $\partial\Omega_i$ for a wavenumber $\kappa_i > 0$ and fundamental solution [1]:

$$G_i(\mathbf{x}, \mathbf{y}) := \frac{\imath}{4} H_0^{(1)}(\kappa_i \|\mathbf{x} - \mathbf{y}\|_2) \tag{6}$$

where $H_0^{(1)}(\cdot)$ is the zeroth order Hankel function of the first kind. We will also refer to them as BI Operators (BIOs).

2.5. Final formulation

Define $\mathbb{V}^{\text{pw}} := \prod_{i=0}^2 \mathbf{V}_i^{\text{pw}}$ and $\widetilde{\mathbb{V}} := \prod_{i=0}^2 \widetilde{\mathbf{V}}_i$. With the above, the variational form of the MTF system is to seek $\boldsymbol{\lambda} = (\boldsymbol{\lambda}^0, \boldsymbol{\lambda}^2, \boldsymbol{\lambda}^2) \in \mathbb{V}^{\text{pw}}$, such that for all $\boldsymbol{\varphi} = (\boldsymbol{\varphi}^0, \boldsymbol{\varphi}^1, \boldsymbol{\varphi}^2) \in \widetilde{\mathbb{V}}$ it holds

$$\langle \mathsf{M}\boldsymbol{\lambda}, \boldsymbol{\varphi}\rangle = \left\langle \mathsf{M}\begin{pmatrix} \boldsymbol{\lambda}^0 \\ \boldsymbol{\lambda}^1 \\ \boldsymbol{\lambda}^2 \end{pmatrix}, \begin{pmatrix} \boldsymbol{\varphi}^0 \\ \boldsymbol{\varphi}^1 \\ \boldsymbol{\varphi}^2 \end{pmatrix} \right\rangle_\times = \left\langle \begin{pmatrix} \mathbf{g}^0 \\ \mathbf{g}^1 \\ \mathbf{g}^2 \end{pmatrix}, \begin{pmatrix} \boldsymbol{\varphi}^0 \\ \boldsymbol{\varphi}^1 \\ \boldsymbol{\varphi}^2 \end{pmatrix} \right\rangle_\times \tag{7}$$

where

$$\mathsf{M} := \begin{pmatrix} \mathsf{A}_0 & -\frac{1}{2}\widetilde{\mathsf{X}}_{01} & -\frac{1}{2}\widetilde{\mathsf{X}}_{02} \\ -\frac{1}{2}\widetilde{\mathsf{X}}_{10} & \mathsf{A}_1 & -\frac{1}{2}\widetilde{\mathsf{X}}_{12} \\ -\frac{1}{2}\widetilde{\mathsf{X}}_{20} & -\frac{1}{2}\widetilde{\mathsf{X}}_{21} & \mathsf{A}_2 \end{pmatrix}, \tag{8}$$

with A_i again denoting block boundary integral operators per subdomain, and $\widetilde{\mathsf{X}}_{ij}$ taking care of transmission conditions per interface.

Structurally, the MTF is amenable to parallelization as each subdomain operator can be sent to different threads. Compared to the original version [17], the difference lies in that the new Galerkin–Petrov system requires local test functions to have restrictions to interfaces Γ_{ij} lying in $\widetilde{H}^{1/2}(\Gamma_{ij}) \times \widetilde{H}^{-1/2}(\Gamma_{ij})$. In practical terms: Dirichlet traces have to become zero at triple points for 2D, while for Neumann data standard bases can be used.

Theorem 1 (*Existence and Uniqueness*). *The local MTF system (7) has a unique solution in* $\mathbb{V}^{\mathrm{pw}}$ *for all* $\mathbf{g}$ *in* $\mathbf{V}_0$.

Proof. This result follows from the same statement for $\mathbb{V} := \prod_{i=0}^{2} \mathbf{V}_i$ in [17]. Extension to piecewise spaces is achieved by duality pairings. □

3. Discretization by spectral elements

3.1. Preliminaries

Define the characteristic function $\mathbf{1}_{\mathcal{O}}$ of a set $\mathcal{O}$ of non-zero measure:

$$\mathbf{1}_{\mathcal{O}}(t) = \begin{cases} 1 & \text{if } t \in \mathcal{O}, \\ 0 & \text{if } t \in \mathcal{O}^c. \end{cases} \tag{9}$$

Set $\hat{\Gamma} := [-1, 1]$. We assume that for each interface Γ_{ij} there is a C^1-parametrization of $\hat{\Gamma}$. Since we assume simply connected domains Ω_i, the union of interfaces renders $\partial\Omega_i$ a closed curved Lipschitz surface. Specifically, for a subdomain boundary $\partial\Omega_i$, we set $h_{ij} : \hat{\Gamma} \to \Gamma_{ij}$ as a positive oriented parametrization of Γ_{ij}. Similarly, we define over $\partial\Omega_j$ a parametrization $h_{ji} : \hat{\Gamma} \to \Gamma_{ij}$. These two parameterizations are required in order to properly orientate subdomains' normals. However, as we will later see, the positive orientation requirement can be dropped as h_{ij}, h_{ji} will be used solely to compute scalar line integrals.

3.2. Spectral elements—Chebyshev polynomials

We will discretize (7) using as both trial and test functions Chebyshev polynomials defined over the parameter space $\hat{\Gamma}$ and mapped onto each interface Γ_{ij}. The Chebyshev polynomials $T_m(x)$ and $U_m(x)$ of the first and second kinds, respectively, are polynomials of degree $m \in \mathbb{N}$, defined in $x \in \hat{\Gamma}$ as:

$$T_m(x) = \cos m\theta \quad \text{and} \quad U_m(x) = \frac{\sin(m+1)\,\theta}{\sin\theta} \tag{10}$$

with $x = \cos\theta$. These satisfy the recurrence relation [22, Form. 2.3.14, 2.3.16]:

$$P_m(x) = 2xP_{m-1}(x) - P_{m-2}(x), \quad m = 2, 3, \ldots, \tag{11}$$

together with initial terms $T_0(x) = 1$, $T_1(x) = x$, $U_0(x) = 1$ and $U_1(x) = 2x$. Furthermore, it holds for $m \in \mathbb{N}$

$$U_m(x) - U_{m-2}(x) = 2T_m(x), \quad m \geq 2, \tag{12}$$

$$T_m'(x) = n\,U_{m-1}(x), \tag{13}$$

$$(\omega(x)U_{m-1}(x))' = -m\omega^{-1}(x)T_m(x), \tag{14}$$

where the weight function $\omega(x)$ is given by

$$\omega(x) := \sqrt{1-x^2}, \quad \text{for } x \in \hat{\Gamma}. \tag{15}$$

Moreover, the T_m are orthogonal with respect to ω^{-1}:

$$\int_{-1}^{1} T_n(x)\,T_m(x)\,\omega^{-1}(x)\,dx = \begin{cases} 0, & n \neq m, \\ \pi/2, & n = m \neq 0, \\ \pi, & n = m = 0. \end{cases} \tag{16}$$

For the second kind Chebyshev polynomials U_m, it holds

$$\int_{-1}^{1} U_n(x)\, U_m(x)\, \omega(x)\, dx = \begin{cases} 0, & n \neq m, \\ \pi/2, & n = m \neq 0. \end{cases} \tag{17}$$

Based on the above, we will construct trial and test function bases for the MTF (7) as piecewise combinations of Chebyshev polynomials mapped onto interfaces Γ_{ij}. For this, we first define canonical bases for trial and test elements restricted over the reference segment $\hat{\Gamma}$, denoted $\hat{\mathbb{T}}_L := \text{span}\{\hat{\boldsymbol{\lambda}}_l\}_{l=0}^{L}$ and $\hat{\mathbb{Q}}_L := \{\hat{\boldsymbol{\varphi}}_l\}_{l=0}^{L}$, respectively, for any $L \in \mathbb{N}$, in the following fashion:

$$\hat{\boldsymbol{\lambda}}_l := (\hat{\lambda}_{\mathrm{D},l}, \hat{\lambda}_{\mathrm{N},l}) = (T_l, U_l) \quad \text{and} \quad \hat{\boldsymbol{\varphi}}_l = (\hat{q}_l, \hat{q}_l), \quad \hat{q}_l := \omega U_l, \ \forall\, l \in \mathbb{N}_0, \tag{18}$$

and where the weight ω forces $\hat{q}_l$ to vanish at the endpoints of $\hat{\Gamma}$. We need to show that sequences generated by $\hat{\mathbb{T}}_L$ and $\hat{\mathbb{Q}}_L$ are dense in $H^{1/2}(\hat{\Gamma}) \times H^{-1/2}(\hat{\Gamma})$ and $\widetilde{H}^{1/2}(\hat{\Gamma}) \times \widetilde{H}^{-1/2}(\hat{\Gamma})$, respectively. For this, we introduce the next auxiliary lemma.

Lemma 1. *Let $f \in L^\infty(\hat{\Gamma})$ and $\delta > 0$. There exists $f_1^\delta \in L^\infty(\hat{\Gamma})$ such that*

$$\left\| f - \omega f_1^\delta \right\|_{L^2(\hat{\Gamma})} \leq \delta. \tag{19}$$

Proof. Let $\epsilon > 0$ and define $f_1^\epsilon := \omega^{-1} f \mathbf{1}_{\omega > \epsilon} \in L^\infty(\hat{\Gamma})$ and $f_2^\epsilon := f \mathbf{1}_{\omega \leq \epsilon}$. Clearly, $f = \omega f_1^\epsilon + f_2^\epsilon$ and it holds

$$\left\| f - \omega f_1^\epsilon \right\|_{L^2(\hat{\Gamma})} = \left\| f_2^\epsilon \right\|_{L^2(\hat{\Gamma})} \leq \sqrt{2\epsilon}\, \|f\|_{L^\infty(\hat{\Gamma})}. \tag{20}$$

Then it suffices to take $\epsilon = \frac{\delta^2}{2\|f\|_{L^\infty}^2}$ to obtain the desired result. □

Proposition 1. *The sequence of subspaces $\{\hat{\mathbb{T}}_L\}_{L\in\mathbb{N}}$ is dense in $H^{1/2}(\hat{\Gamma}) \times H^{-1/2}(\hat{\Gamma})$ and $\{\hat{\mathbb{Q}}_L\}_{L\in\mathbb{N}}$ in $\widetilde{H}^{1/2}(\hat{\Gamma}) \times \widetilde{H}^{-1/2}(\hat{\Gamma})$.*

Proof. Density of subspaces $\{\hat{\mathbb{T}}_L\}_{L\in\mathbb{N}}$ in $H^{1/2}(\hat{\Gamma}) \times H^{-1/2}(\hat{\Gamma})$ follows from the density of polynomials onto the space of continuous functions (Weierstrass' theorem), and by invoking Sobolev embeddings [1, Section 2.5]. Hence, we focus on proving the statement for $\hat{\mathbb{Q}}_L$ and particularly on the properties of $\hat{Q}_L := \text{span}\{\hat{q}_l\}_{l=0}^{L}$. Density of $\hat{Q}_L$ in $\widetilde{H}^{1/2}(\hat{\Gamma})$ follows from the Chebyshev expansion and density results [23, Section 4.5]. Thus, we are left to tackle the density $\hat{Q}_L$ in $\widetilde{H}^{-1/2}(\hat{\Gamma})$.

Let $\epsilon > 0$ and $f, g \in \mathcal{D}(\hat{\Gamma})$. By density arguments, it is sufficient to show that there exists an $L \in \mathbb{N}$ such that for a certain $f_L \in \hat{Q}_L := \text{span}\{\hat{q}_l\}_{l=0}^{L}$ it holds

$$\|f - f_L\|_{\widetilde{H}^{-1/2}(\hat{\Gamma})} = \sup_{g\in\mathcal{D}(\hat{\Gamma})} \frac{\langle f - f_L, g\rangle}{\|g\|_{H^{1/2}(\hat{\Gamma})}} \leq \epsilon. \tag{21}$$

Since $f_L \in Q_L$, $f_L = \omega f_L^*$ with $f_L^* \in \text{span}\{U_l\}_{l=0}^{L}$. Thus, by continuity of the duality product

$$\left|\langle f - \omega f_L^*, g\rangle\right| \leq \left\|\omega^{1/2}(f - \omega f_L^*)\right\|_{L^2(\hat{\Gamma})} \left\|\omega^{-1/2} g\right\|_{L^2(\hat{\Gamma})}. \tag{22}$$

On one hand, it holds [24,25]

$$\left\|\omega^{-1/2} g\right\|_{L^2(\hat{\Gamma})} \leq C\, \|g\|_{H^{1/2}(\hat{\Gamma})}, \tag{23}$$

while

$$\left\|\sqrt{\omega}(f - \omega f_L^*)\right\|_{L^2(\hat{\Gamma})} \leq \left\|f - \omega f_L^*\right\|_{L^2(\hat{\Gamma})}. \tag{24}$$

Set $\delta = \frac{\epsilon}{2C}$. By Lemma 1, there exists a $f_1^\delta \in L^\infty(\hat{\Gamma})$ such that

$$\left\|(f - \omega f_L^*)\right\|_{L^2(\hat{\Gamma})} \leq \left\|f - \omega f_1^\delta\right\|_{L^2(\hat{\Gamma})} + \left\|\omega(f_L^* - f_1^\delta)\right\|_{L^2(\hat{\Gamma})} \leq \frac{\epsilon}{2C} + \left\|f_L^* - f_1^\delta\right\|_{L^2(\hat{\Gamma})}. \tag{25}$$

By density of continuous functions in $L^2(\hat{\Gamma})$ and again Weierstrass' theorem, there is a $L \in \mathbb{N}$ then such that

$$\left\|f_L^* - f_1^\delta\right\|_{L^2(\hat{\Gamma})} \leq \epsilon/2C, \tag{26}$$

from where

$$\left\|f - \omega f_L^*\right\|_{L^2(\hat{\Gamma})} \leq \frac{\epsilon}{C}. \tag{27}$$

By replacing the above in (24) and using (23), (22) becomes

$$|\langle f - f_L, g\rangle| = \left|\langle f - \omega f_L^*, g\rangle\right| \leq \epsilon\, \|g\|_{H^{1/2}(\hat{\Gamma})}, \tag{28}$$

from where (21) follows. □

Next, we use the family $\{\hat{\mathbb{T}}_L\}_{L\in\mathbb{N}}$ to define approximation bases for the spaces $\mathbf{V}_i^{\mathrm{pw}}$ of unknown Dirichlet and Neumann traces by using the mapping h_{ij} introduced in Section 3.1. Specifically, we define at each interface Γ_{ij}, the basis functions $\boldsymbol{\lambda}_m^{ij} := \hat{\boldsymbol{\lambda}}_m \circ h_{ij}^{-1}$, $m \in \mathbb{N}_0$, such that, over each subdomain boundary $\partial\Omega_i$, we build functions:

$$\boldsymbol{\lambda}_m^i := \sum_{j\in\Lambda_i} \boldsymbol{\lambda}_m^{ij} \mathbf{1}_{\Gamma_{ij}}. \tag{29}$$

As expected, these functions are piecewise polynomials of degree L over $\partial\Omega_i$. Analogously, we use $\{\hat{\mathbb{Q}}_L\}_{L\in\mathbb{N}}$ to devise suitable test functions. First, set $\boldsymbol{\varphi}_l^{ij} := \hat{\boldsymbol{\varphi}}_l \circ h_{ij}^{-1}$, $l \in \mathbb{N}_0$, then

$$\boldsymbol{\varphi}_l^i := \sum_{j\in\Lambda_i} \boldsymbol{\varphi}_l^{ij} \mathbf{1}_{\Gamma_{ij}}. \tag{30}$$

Notice that the test functions satisfy

$$\boldsymbol{\varphi}_l^i(\mathbf{y}) = 0, \quad \forall\, \mathbf{y} \in \partial\Gamma_{ij},\ j \in \Lambda_i. \tag{31}$$

Although this property is required for functions conforming in $\widetilde{H}^{1/2}(\Gamma_{ij})$, it has a more practical use: it improves the computation of the discretized integral operators entries, as will be seen in Section 3.3.

Provided with the above definitions, we are set to define the discrete spaces for trial and test functions over $\partial\Omega_i$ used to approximate solutions of (7) for $N_i \in \mathbb{N}$:

$$\mathbf{V}_{i,N_i}^{\mathrm{pw}} := \mathrm{span}\{\boldsymbol{\lambda}_m^i\}_{m=0}^{N_i} \quad \text{and} \quad \tilde{\tilde{\mathbf{V}}}_{i,N_i} := \mathrm{span}\{\boldsymbol{\varphi}_l^i\}_{l=0}^{N_i}. \tag{32}$$

For $\mathbf{N} = (N_0, N_1, N_2) \in \mathbb{N}^3$, we set Cartesian product spaces

$$\mathbb{V}_{\mathbf{N}}^{\mathrm{pw}} := \prod_{i=0}^{2} \mathbf{V}_{i,N_i}^{\mathrm{pw}} \quad \text{and} \quad \tilde{\tilde{\mathbb{V}}}_{\mathbf{N}} := \prod_{i=0}^{2} \tilde{\tilde{\mathbf{V}}}_{i,N_i}. \tag{33}$$

Proposition 2. *Let $N \in \mathbb{N}$, and $\mathbf{N} = (N, N, N) \in \mathbb{N}^3$, then $\left\{\mathbb{V}_{\mathbf{N}}^{\mathrm{pw}}\right\}_{N\in\mathbb{N}}$ and $\{\tilde{\tilde{\mathbb{V}}}_{\mathbf{N}}\}_{N\in\mathbb{N}}$ are dense sequences of subspaces of $\mathbb{V}^{\mathrm{pw}}$ and $\tilde{\tilde{\mathbb{V}}}$, respectively.*

Proof. Follows directly from Proposition 1. □

3.3. BIOs approximation—computational strategy

Armed with the above results, we now focus on the construction of the Galerkin–Petrov matrices originated from the MTF presented in Section 2.5. Particular attention is made to the approximation of the BI kernels and acceleration via FFT techniques [26,8]. We need to compute integrals of the canonical form:

$$I_{\mathsf{L}}[m, l] = \left\langle \mathsf{L}\hat{\lambda}_m, \hat{q}_l \right\rangle = \int_{\hat{\Gamma}} \int_{\hat{\Gamma}} F_{\mathsf{L}}(s, t) T_m(s) \omega(t) U_l(t) ds dt, \tag{34}$$

where L is any of the BIOs and F_{L} represents the associated kernel including mappings required to push interfaces Γ_{ij} onto $\hat{\Gamma}$. The strategy followed relies on two steps:

1. **Kernel approximation**. We first approximate the kernel F_{L} as a degenerate kernel using Chebyshev polynomials. Since Chebyshev polynomials can be directly be connected with Fourier series [26, Chapter 3], one can make use of the FFT to compute coefficients $g_n(t)$ such that

$$F(s, t) \approx \sum_{n=0}^{N_c} g_n(t) T_n(s), \tag{35}$$

for a suitable choice of N_c. This expression converges fastly for $t \neq s$. Alternatively, using (12) the approximation (35) can be rewritten in terms of second kind Chebyshev polynomials as

$$F(s, t) \approx \sum_{n=0}^{N_c} f_n(t) U_n(s). \tag{36}$$

A discussion on these numerical kernel approximation is given in Section 4.1.

2. **Orthogonality**. By applying the orthogonality properties of Chebyshev polynomials, one can quickly obtain expressions of the form:

$$I_{\mathrm{L}}[m, l] \approx \frac{\pi}{2} c_l \int_{-1}^{+1} f_m(t) T_m(t) dt \tag{37}$$

which can be computed by either the trapezoidal method or Gauss–Legendre quadrature.

Parallel to the above, one should be aware of the existence of two different singular behaviors in the integrands depending on whether the interfaces Γ_{ij} and Γ_{ik} coincide or not, i.e. for $j, k \in \Lambda_i$. Specifically,

- If $j \neq k$, the singularity occurs only at $s = t = \pm 1$, where the Chebyshev expansion loses accuracy.
- If $j = k$, singularities lie on the line $t = s$ with $t, s \in \hat{\Gamma}$. In this case, we follow standard regularization techniques [27] to extract the singularity.

3.3.1. Single layer operator (V_i) computation

The singular layer BIO maps Neumann trace data to Dirichlet one. Given the piecewise structure of our approximation bases, the discretization of the bilinear form associated to the single layer becomes, for $m, l \in \mathbb{N}_0$,

$$I_{\mathsf{V}_i}[l, m] := \left\langle \mathsf{V}_i \lambda^i_{\mathrm{N},l}, \varphi^i_{\mathrm{D},m} \right\rangle_{\partial\Omega_i} = \left\langle \mathsf{V}_i \lambda^i_{\mathrm{N},l}, \sum_{j \in \Lambda_i} q^{ij}_m \mathbf{1}_{\Gamma_{ij}} \right\rangle_{\partial\Omega_i} = \sum_{j \in \Lambda_i} \left\langle \mathsf{V}_i \lambda^i_{\mathrm{N},l}, q^{ij}_m \right\rangle_{\Gamma_{ij}}, \tag{38}$$

We have defined $q^{ij}_m := \hat{q}_m \circ h_i j^{-1}$. At the same time,

$$\mathsf{V}_i \lambda^i_{\mathrm{N},l}(\mathbf{x}) = \left\langle G_i(\mathbf{x}, \cdot), \sum_{k \in \Lambda_i} \lambda^{ik}_{\mathrm{N},l} \mathbf{1}_{\Gamma_{ik}} \right\rangle_{\partial\Omega_i} = \sum_{k \in \Lambda_i} \left\langle G_i(\mathbf{x}, \cdot), \lambda^{ik}_{\mathrm{N},l} \right\rangle_{\Gamma_{ik}}. \tag{39}$$

To be even more explicit, (38) reads,

$$I_{\mathsf{V}_i}[l, m] = \sum_{j \in \Lambda_i} \sum_{k \in \Lambda_i} \left\langle \left\langle G_i(\mathbf{x}, \cdot), \lambda^{ik}_{\mathrm{N},l} \right\rangle_{\Gamma_{ik}}, q^{ij}_m \right\rangle_{\Gamma_{ij}}. \tag{40}$$

We study the summands $I^{jk}_{\mathsf{V}_i}[l, m] := \left\langle \left\langle G_i(\mathbf{x}, \cdot), \lambda^{ik}_{\mathrm{N},l} \right\rangle_{\Gamma_{ik}}, q^{ij}_m \right\rangle_{\Gamma_{ij}}$. By continuity, we can write

$$I^{jk}_{\mathsf{V}_i}[l, m] = \int_{\hat{\Gamma}} \int_{\hat{\Gamma}} G_i \left(\left\| h_{ij}(s) - h_{ik}(t) \right\|_2 \right) U_l(t) \omega(s) U_m(s) \left\| h'_{ik}(t) \right\| \left\| h'_{ij}(s) \right\| ds dt. \tag{41}$$

Case $j \neq k$. The term $G_i \left(\left\| h_{ij}(s) - h_{ik}(t) \right\|_2 \right)$ presents at most two singularities corresponding to the end points, i.e. $t = s = \pm 1$. For all $t \in (-1, 1)$, Weierstrass' theorem [26, Chapter 6] guarantees uniform convergence of the Chebyshev expansion,

$$G_i \left(\left\| h_{ij}(s) - h_{ik}(t) \right\|_2 \right) \left| h'_{ij}(s) \right| \approx \sum_{n=0}^{N_c} g_n(t) T_n(s), \quad N_c \in \mathbb{N}, \tag{42}$$

converges uniformly to the left hand side, where coefficients $g_n(t)$ are computed by the FFT algorithm. By (12), series (42) can be written in terms of second kind Chebyshev polynomials, with coefficients $f_n(t)$, and by orthogonality property (17), one eliminates one of the integrals in (41) to retrieve

$$I^{jk}_{\mathsf{V}_i}[l, m] \approx \int_{-1}^{1} \frac{\pi}{2} f_m(t) U_l(t) \left\| h'_{ik}(t) \right\| dt, \quad \text{for } j \neq k. \tag{43}$$

This last integral is obtained via quadrature as mentioned before. Note that coefficients $f_m(t)$ are only required for interior points, i.e. $t \in (-1, 1)$.

Case $j = k$. To avoid this difficulty, the kernel G_i is regularized. Let us recall the kernel corresponding to the Laplacian problem (null frequency, $\kappa_i = 0$):

$$G_0 \left(\|\mathbf{x} - \mathbf{y}\|_2 \right) = -\frac{1}{2\pi} \log \|\mathbf{x} - \mathbf{y}\|_2. \tag{44}$$

By using a Taylor expansion together with the series representation for the Hankel function to represent G_i [22, Formula 9.1.3], one can deduce that for a C^1-parametrization h_{ij} of the interface, the following kernel subtraction is a continuous

function [28, Section 2.4], i.e.

$$H_i(t,s) := G_i\left(\left\|h_{ij}(s) - h_{ij}(t)\right\|_2\right) - G_0(|s-t|) \in C^0(\hat{\Gamma}\times\hat{\Gamma}). \tag{45}$$

This property leads to the splitting $I_{V_i}[l,m] = I^1_{V_i}[l,m] + I^2_{V_i}[l,m]$ with

$$I^1_{V_i}[l,m] := \int_{\hat{\Gamma}}\int_{\hat{\Gamma}} H_i(t,s)U_l(t)\omega(s)U_m(s)\left\|h'_{ij}(s)\right\|\left\|h'_{ik}(t)\right\| dsdt, \tag{46}$$

$$I^2_{V_i}[l,m] := \int_{\hat{\Gamma}}\int_{\hat{\Gamma}} G_0(|s-t|)U_l(t)\omega(s)U_m(s)\left\|h'_{ij}(s)\right\|\left\|h'_{ik}(t)\right\| dsdt. \tag{47}$$

The regularity of $H_i(t,s)\left\|h'_{ij}(s)\right\|$ allows uniform convergence for the associated Chebyshev expansion, and thus, the computation of $I^1_{V_i}$ is given by quadrature formula as in (37).

To calculate $I^2_{V_i}$, we recall that the kernel G_0 can be written as a series of Chebyshev polynomials [23, Theorem 4.4]:

$$G_0(|t-s|) = \frac{1}{2\pi}\log 2 + \sum_{n=1}^{\infty}\frac{1}{n\pi}T_n(t)T_n(s), \quad s\neq t\in\hat{\Gamma}. \tag{48}$$

Thus, we can quickly derive the following expansion:

$$G_0(|s-t|)\left\|h'_{ij}(s)\right\| \approx \sum_{n=0}^{\infty} v_n(t)U_n(s), \tag{49}$$

with final computation of $I^2_{V_i}$ again carried out using (37).

3.3.2. Double layer operators (K_i, K'_i) computation

We only consider the case of K_i as similar arguments hold for its adjoint. Discretization of bilinear forms for $m, l\in\mathbb{N}_0$ are

$$I_{\mathsf{K}_i}[l,m] := \left\langle \mathsf{K}_i\lambda^i_{\mathrm{D},l}, \varphi^i_{\mathrm{N},m}\right\rangle_{\partial\Omega_i} = \left\langle \mathsf{K}_i\lambda^i_{\mathrm{D},l}, \sum_{j\in\Lambda_i} q^{ij}_m \mathbf{1}_{\Gamma_{ij}}\right\rangle_{\partial\Omega_i} = \sum_{j\in\Lambda_i}\left\langle \mathsf{K}_i\lambda^i_{\mathrm{D},l}, q^{ij}_m\right\rangle_{\Gamma_{ij}}. \tag{50}$$

Again, the operator action on $\lambda^i_{\mathrm{D},l}$ can be written as

$$\mathsf{K}_i\lambda^i_{\mathrm{D},l}(\mathbf{x}) = \left\langle \frac{\partial G_i}{\partial n_{\mathbf{y}}}(\mathbf{x},\cdot), \sum_{k\in\Lambda_i}\lambda^{ik}_{\mathrm{D},l}\mathbf{1}_{\Gamma_{ik}}\right\rangle_{\partial\Omega_i} = \sum_{k\in\Lambda_i}\left\langle \frac{\partial G_i}{\partial n_{\mathbf{y}}}(\mathbf{x},\cdot), \lambda^{ik}_{\mathrm{D},l}\right\rangle_{\Gamma_{ik}}, \tag{51}$$

where the normal derivative of the Green kernel is

$$\frac{\partial G_i}{\partial n_{\mathbf{y}}} = -\kappa_i H^{(1)}_1(\kappa_i\|\mathbf{x}-\mathbf{y}\|_2)\frac{(\mathbf{y}-\mathbf{x})\cdot\mathbf{n}_y}{\|\mathbf{x}-\mathbf{y}\|_2}, \tag{52}$$

with $\mathbf{n}_y$ being the outward normal vector to the interface at the point y.

Case $j\neq k$. For double layer operators, singularities at $t=s=\pm1$ are stronger than for the single layer case, i.e. compare $H^{(1)}_1(\kappa_i\|x-y\|_2)\sim\frac{1}{\|x-y\|_2}$ to $H^{(1)}_0(\kappa_i\|x-y\|_2)\sim\log\|x-y\|_2$, and thus, the approximation by Chebyshev polynomials is much worse when approaching the corners. Luckily, thanks to the weighted test function this singularities are smoothened yielding a precise approximation of I_{K_i} and $I_{\mathsf{K}'_i}$ (see Table 1).

Case $j=k$. To be able to apply to Chebyshev series approximation, the kernel requires to be continuous, which is shown in the following proposition:

Proposition 3 (*Lemma 2.2.14 in [1]*). *Let* $\mathbf{n}$ *denote the exterior normal to* Ω_i. *If* $\mathbf{n}$ *is continuous over* Γ_{ij}, *then there exists a bounded constant* $c_{\mathbf{n}}>0$ *such that*

$$\left|(\mathbf{y}-\mathbf{x})\cdot\mathbf{n}_y\right| \leq c_{\mathbf{n}}\|\mathbf{y}-\mathbf{x}\|_2^2, \quad \mathbf{x}\neq\mathbf{y}\in\Gamma_{ij}. \tag{53}$$

Thus, it is straightforward to show that if the interface Γ_{ij} is a C^1-curve then the double layer BIO kernel is continuous, and can be approximated by,

$$\frac{\partial G_i}{\partial n_{\mathbf{y}}}\left|h'_{ij}(s)\right| \approx \sum_{n=0}^{Nc} k_n(t)U_n(s) \tag{54}$$

and we can proceed as sketched at the beginning of Section 3.3.

Table 1
Kernel approximation performances for different values of N_c.

t	e^V_{Cheb}	$e_{I_V}[0,0]$	e^K_{Cheb}	$e_{I_K}[0,0]$
(a) $N_c = 128$				
0.9	10^{-15}		10^{-15}	
0.99	10^{-7}		10^{-8}	
0.9999	10^{-3}	10^{-14}	10^{-3}	10^{-12}
$1-10^{-6}$	10^{-2}		10^{-1}	
$1-10^{-8}$	10^{-2}		10^{0}	
(b) $N_c = 1280$				
0.9	10^{-15}		10^{-15}	
0.99	10^{-14}		10^{-14}	
0.9999	10^{-8}	10^{-14}	10^{-7}	10^{-12}
$1-10^{-6}$	10^{-4}		10^{-1}	
$1-10^{-8}$	10^{-2}		10^{0}	
(c) $N_c = 12\,800$				
0.9	10^{-15}		10^{-15}	
0.99	10^{-14}		10^{-14}	
0.9999	10^{-11}	10^{-14}	10^{-11}	10^{-12}
$1-10^{-6}$	10^{-9}		10^{-6}	
$1-10^{-8}$	10^{-6}		10^{0}	

3.3.3. Hypersingular operator (W_i) computation

Here we carry out the same piecewise summation over interfaces Γ_{ij} and recast the problem in terms of single layer operator as follows. First, recall that for a curve Γ piecewise smooth in $\mathbb{R}^2$ with unitary normal vector $\mathbf{n}$, and a $C^1(I)$-function defined on a neighborhood I of Γ, $f : I \to \mathbb{R}$, the curl operator reads

$$\operatorname{curl} f(\mathbf{x}) := n^1(\mathbf{x})\partial_2 f(\mathbf{x}) - n^2(\mathbf{x})\partial_1 f(\mathbf{x}), \quad \mathbf{x} \in \Gamma. \tag{55}$$

We then invoke the following result:

Proposition 4 (*Theorem 6.15 in [29]*)**.** *Let Γ be a sufficiently smooth, bounded curve in $\mathbb{R}^2$ and let g, f be $C^1(\Gamma)$-functions such that $g(\mathbf{y}) = 0$ for all $\mathbf{y} \in \partial\Gamma$. Then it holds:*

$$\langle \mathsf{W}_i f, g\rangle_{\partial\Omega_i} = \langle \mathsf{V}_i \operatorname{curl} f, \operatorname{curl} g\rangle_{\partial\Omega_i} - \kappa_i^2 \langle \mathbf{n}_{\mathbf{x}} \cdot \mathbf{n}_{\mathbf{y}} \mathsf{V}_i f, g\rangle_{\partial\Omega_i} - f \int_{\Gamma} G_i(\|\mathbf{x}-\mathbf{y}\|) \operatorname{curl} g(\mathbf{y}) d\Gamma_{\mathbf{y}} \Big|_{\mathbf{x}\in\partial\Gamma}. \tag{56}$$

Thus, for $I_{\mathsf{W}_i}[l, m]$ we can also obtain a Fourier–Chebyshev series expansion. We establish explicit formulas for $\operatorname{curl} \hat{\lambda}_{\mathrm{D},m}$ and $\operatorname{curl} \hat{q}_l$ via the polynomial properties presented in Section 3.2:

$$\operatorname{curl} \hat{\lambda}_{\mathrm{D},m} = T'_m = mU_{m-1}, \tag{57}$$

$$\operatorname{curl} \hat{q}_l = (\omega U_l)' = -\omega^{-1} T_{l+1}. \tag{58}$$

Since now test functions are expressed in terms of first kind Chebyshev polynomials, orthogonality relation (16) allows direct use of the Chebyshev expansion of the kernel. Note that the term,

$$\hat{\lambda}_{\mathrm{D},m} \int_{\Gamma_{ij}} G_i(\|\mathbb{x} - \mathbb{y}\|) \operatorname{curl} q_l^{ij}(\mathbb{y}) d\Gamma \Big|_{x\in\partial\Gamma_{ij}} \tag{59}$$

is not accurate close to the corners ($t = \pm 1$) when $j \neq k$. To circumvent this issue, we observe that a corner belongs to two interfaces and, instead of considering the point on the interface Γ_{ij}, we take it on Γ_{ik}. This leads back to the case $j = i$ and kernel regularization is used to compute the required coefficient.

4. Numerical results

We now present numerical simulations for a two-dimensional scatterer. We first examine the range of validity of our numerical approximations for the BIOs, then consider error convergence for fixed wavenumbers and with respect to a frequency sweep. Finally, we study the effect of preconditioning for iterative solvers.

The geometry considered is illustrated in Fig. 2, and it consists of three domains: $\Omega_0 := \{\mathbf{x} \in \mathbb{R}^2, \|\mathbf{x}\|_2 > 1\}$, $\Omega_1 := \{\mathbf{x} \in \mathbb{R}^2, \|\mathbf{x}\|_2 < 1, x_1 < 0\}$, and $\Omega_2 := \{\mathbf{x} \in \mathbb{R}^2, \|\mathbf{x}\|_2 < 1, x_1 > 0\}$. This simple case contains all the difficulties portraying Lipschitz domains with sharp corners. The experiments were performed on MATLAB 2009b, 64-bit, running on a GNU/Linux desktop machine with 3.40 GHz CPU and 32 GB RAM. The discretization of the operators is computed by a MEX-C library.

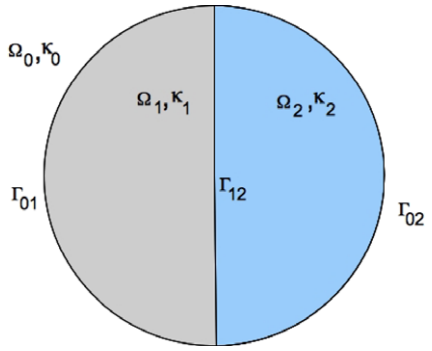

Fig. 2. Canonical geometry used to test the spectral MTF method.

CPU times to compute the MTF system of moderate to high frequency (κ from 10 to 100) range between a few seconds to less than one hour.

Heuristically, the parameter used in the degenerate expansion of the kernels is given by $N_c = 2\text{ceil}(3N + \max \kappa_i) + 128$. Also observe that when considering N for the number of degrees of freedom, $2N + 1$ trial and test functions are considered.

4.1. BIOs numerical approximation

Let us define the following errors for different values of $N_c \in \mathbb{N}$ for a given $t \in \hat{\Gamma}$ and interface Γ_{ik}:

$$e^{\mathsf{V}}_{\text{Cheb}}(t) := \left\| G_k\left(\|\mathbf{x}(t) - \mathbf{y}(s)\|\right) \left|h'_{ik}(s)\right| - \sum_{n=0}^{N_c} g_n(t) T_n(s) \right\|_{L^2(\hat{\Gamma})},$$

$$e^{\mathsf{K}}_{\text{Cheb}}(t) := \left\| \frac{\partial G_i}{\partial n}\left(\|\mathbf{x}(t) - \mathbf{y}(s)\|\right) \left|h'_{ik}(s)\right| - \sum_{n=0}^{N_c} g_n(t) T_n(s) \right\|_{L^2(\hat{\Gamma})}.$$

The errors of the discretized Galerkin–Petrov operators for entries $I_{\mathsf{L}}[m, l]$ are found by integrating over the next interface Γ_{ij}, and we drop the superscript ij in (41):

$$e_{I_{\mathsf{V}}}[m, l] := \left| I^{\text{Cheb}}_{\mathsf{V}}[m, l] - I^{\text{quad}}_{\mathsf{V}}[m, l] \right|,$$

$$e_{I_{\mathsf{K}}}(m, l) := \left| I^{\text{Cheb}}_{\mathsf{K}}[m, l] - I^{\text{quad}}_{\mathsf{K}}(m, l] \right|$$

where $I^{\text{Cheb}}_{\mathsf{V}}$, $I^{\text{Cheb}}_{\mathsf{K}}$ are the approximations of I_{V} and I_{K} using the method described in Sections 3.3.1 and 3.3.2, respectively. Values $I^{\text{quad}}_{\mathsf{V}}$, $I^{\text{quad}}_{\mathsf{K}}$ are approximations obtained using an expensive adaptative quadrature scheme. Results for a few cases are given in Table 1. The good accuracy of the approximation for $I^{\text{Cheb}}_{\mathsf{V}}$, $I^{\text{Cheb}}_{\mathsf{K}}$ arises from the smoothening behavior of the weighted test functions.

4.2. Symmetric configuration

We study the case of one penetrable obstacle as described in Fig. 2 with equal interior wavenumbers $\kappa_1 = \kappa_2$, and varying exterior wavenumber κ_0. Under these conditions, the exact solution is provided by means of Mie series [30, Section 3.1.5] which are used to validate the model.

Fig. 3 depicts convergence rates in different norms pointing out at a maximum number of degrees of freedom after which, no further convergence is achieved. This is due to the numerical approximation of the BIOs and is bounded by machine precision in the best case. In fact, the total number of trial and test functions required to reach a given accuracy can be derived from asymptotics of the underlying Mie series. From these figures, one can observe that this number is not completely linear with the wavenumber, e.g., for an error of 10^{-4}, $N \approx 12$ at $\kappa_0 = 10$, $N \approx 45$ at $\kappa_0 = 50$ and $N \approx 80$ at $\kappa_0 = 100$. More details about the number of degrees of freedom is given in Section 4.4. On the other hand, the error derived from the weak Calderón identities in Fig. 6 is defined as the Euclidean norm of the vector $v = \langle 2A_i\lambda^i, \phi^i\rangle - \langle \lambda^i, \phi^i\rangle$.

4.3. Asymmetric configuration

Subdomains Ω_1 and Ω_2 portrayed in Fig. 2 are now given different wavenumbers, $\kappa_1 = 50$ and $\kappa_2 = 1$, with exterior wavenumber set to $\kappa_0 = 100$. In this configuration, solutions cannot be computed via Mie series nor is there any analytic solution available. To validate the model, we check whether jump relations (3b) and (3c) are fulfilled.

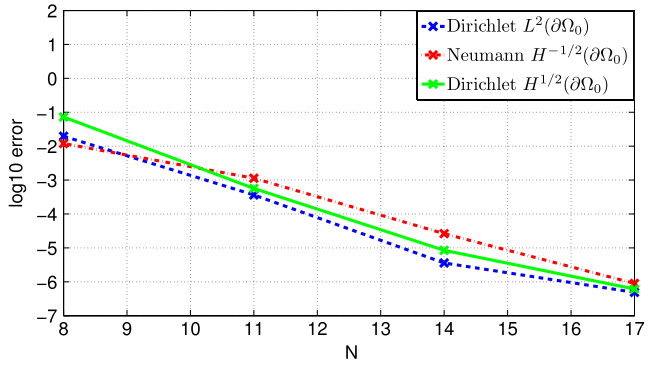

(a) $\kappa_0 = 10$.

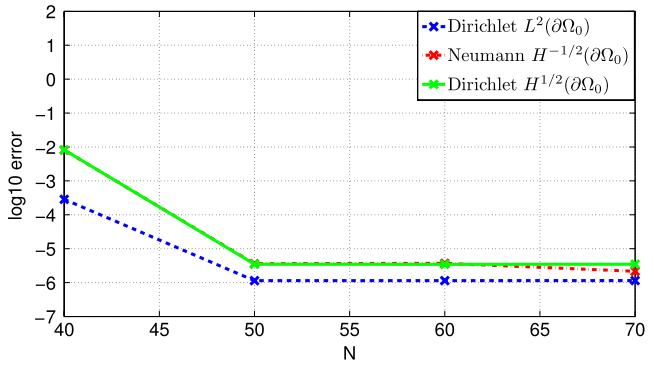

(b) $\kappa_0 = 50$.

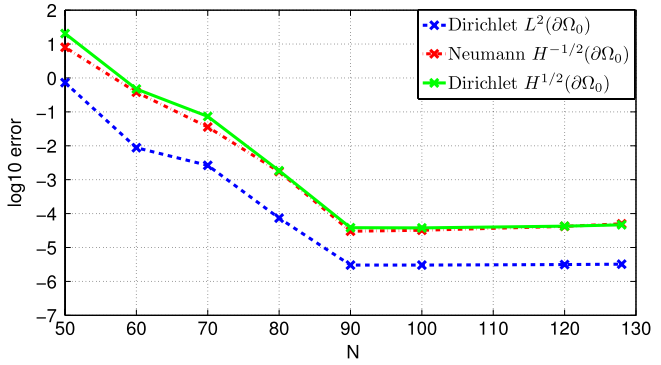

(c) $\kappa_0 = 100$.

Fig. 3. Error convergence for the exterior trace in different norms for the Dirichlet and Neumann traces $(\lambda_0^{\mathrm{D}}, \lambda_0^{\mathrm{N}})$ on $\partial\Omega_0$ for two half-circles with $\kappa_1 = \kappa_2 = 1$ and different values of κ_0. The impinging plane wave comes at an angle $\theta = 0°$ but similar behaviors are obtained for other angles. Exact traces are obtained via Mie series.

Figs. 4 and 5 show traces defined on each interface for the mentioned case. Expected jump relations (3b) and (3c) are satisfied and their corresponding error is of magnitude 10^{-12} in L^2-norm. Note that Neumann traces are not continuous at the triple points, e.g., at angles $-90°, 90°, 270°$, which are taken into account by the discontinuous trial functions belonging to $\mathbf{V}_0^{\mathrm{pw}}$.

4.4. Error convergence frequency analysis

Until now we have only verified that the model works for different wavenumbers. However, for most real applications, one usually fixes physical parameters and seeks for solutions over a frequency range. To illustrate this, we recall the wavenumber definition for the electromagnetic case per subdomain, $\kappa_i = \omega_0\sqrt{\epsilon_i\mu_i}$, where ϵ_i and μ_i are the dielectric and permeability constants, respectively, and ω_0 is the radial frequency of excitation.

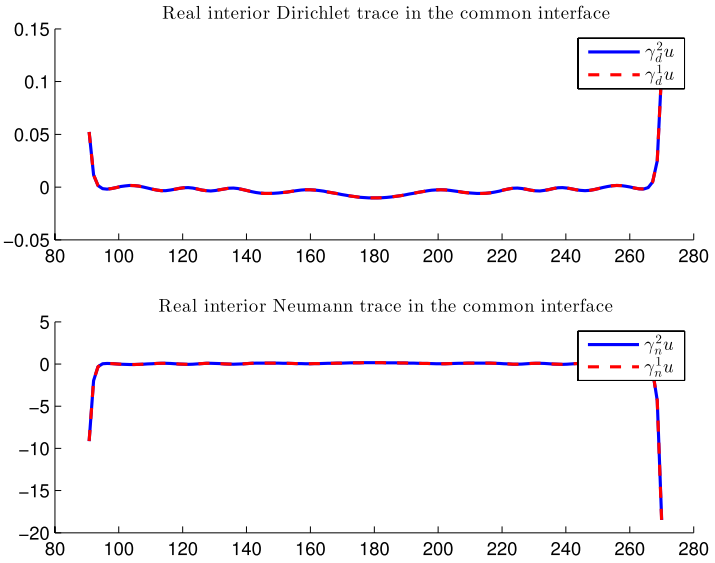

Fig. 4. Dirichlet and Neumann traces ($\lambda_{1,2}^{\mathrm{D}}$, $\lambda_{1,2}^{\mathrm{N}}$) on the interface Γ_{12}, one taken from Ω_1 (dashed-red), and another one taken from Ω_2 (blue). The values of the wavenumbers are $\kappa_0 = 100$, $\kappa_1 = 50$ and $\kappa_2 = 1$ for an impinging plane wave at an angle $\theta = 0°$. The x-axis represents the coordinate parametrization and the y-axis represents the real part of the traces in arbitrary units. (For interpretation of the references to color in this figure legend, the reader is referred to the web version of this article.)

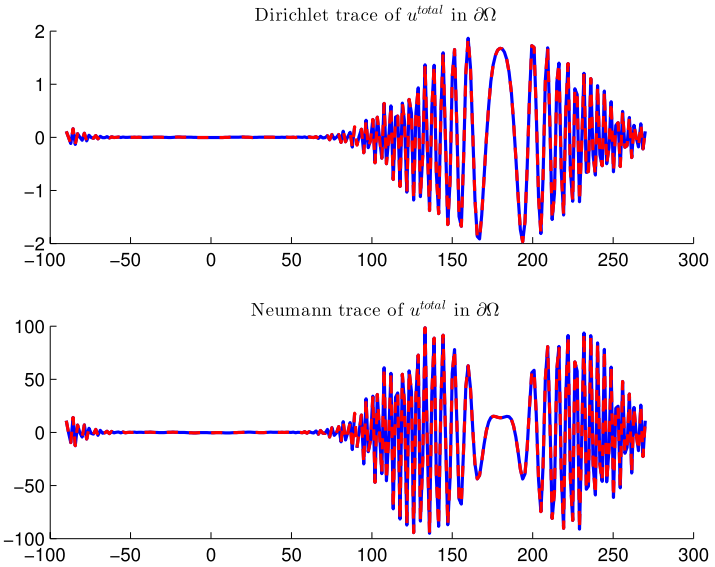

Fig. 5. Dirichlet and Neumann traces at interfaces Γ_{01} and Γ_{02}, one with the incident field included taken from outside (Ω_0) in dashed-red, and another one taken from inside $\Omega_{1,2}$ in blue. Wavenumber values are $\kappa_0 = 100$, $\kappa_1 = 50$ and $\kappa_2 = 1$, for an impinging plane wave with angle $\theta = 0$. The x-axis represents the coordinate parametrization and the y-axis represents the real part of the traces in arbitrary unit. (For interpretation of the references to color in this figure legend, the reader is referred to the web version of this article.)

To simplify our analysis, we set permeabilities $\mu_i = 1$, for all $i = 0, 1, 2$, and set $\epsilon_0 = 1$ so that wavenumbers become $\kappa_0 = \omega_0$, $\kappa_i = \kappa_0\sqrt{\epsilon_i}$, $i \in \{1, 2\}$. We now fix ϵ_i and compute the approximation error for a range of values of κ_0. For every κ_0, we need to determine the number of test and trial functions. Based on the truncation of Mie series [30], for the symmetric case we tried three different rules with their specifications given in Fig. 6.

We observe that for the symmetric case the three rules have a similar behavior so we choose the rule minimizing the number of degrees of freedom, $2N_i+1 = 1.1\kappa_i+7$. We repeat the same experiment but now for an asymmetric arrangement, $\epsilon_1 = 2$, $\epsilon_2 = 3$, for which results are displayed in Fig. 7. As can be seen, only the rule $2N_i + 1 = 1.1 \max_i\{\kappa_i\} + 7$ works for all the cases but is not optimal in terms of degrees of freedom. Since we lack adequate Mie series this deserves future investigation.

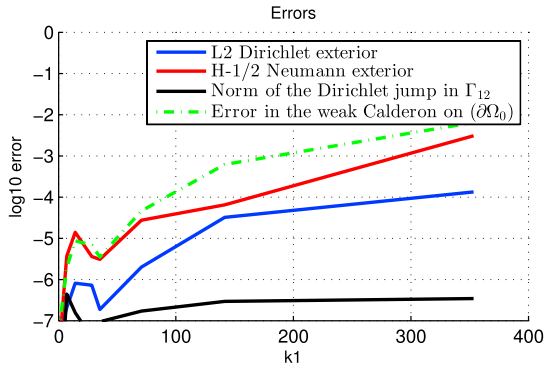

(a) Rule 1: $2N_i + 1 = 1.4\kappa_i + 7$.

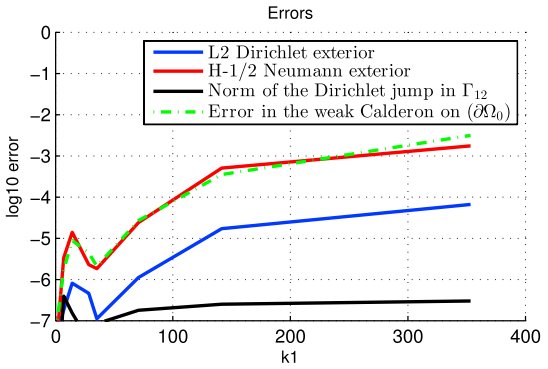

(b) Rule 2: $2N_i + 1 = 1.1\kappa_i + 7$.

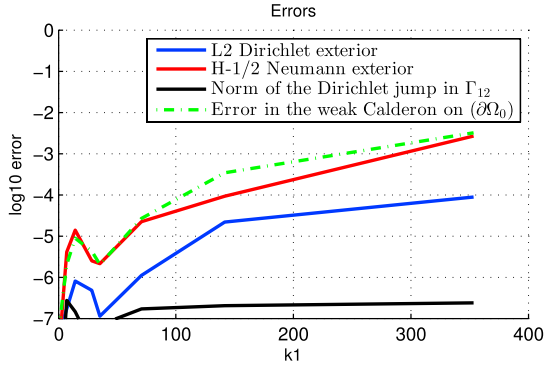

(c) Rule 3: $2N_i + 1 = 1.1 \max_i\{\kappa_i\} + 7$.

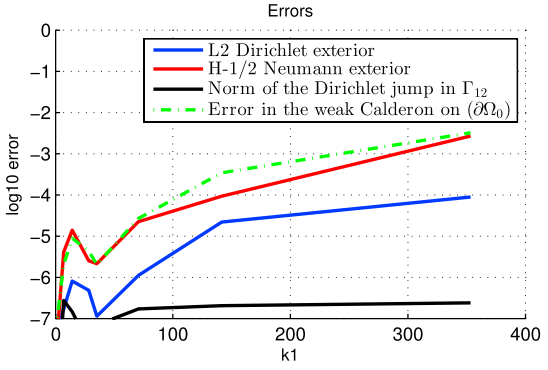

(d) Rule 4: $2N_i + 1 = 1.4 \max_i\{\kappa_i\} + 7$.

Fig. 6. Error performance versus wavenumber $\kappa_0 \in [0, 250]$ in different norms for the symmetric case.

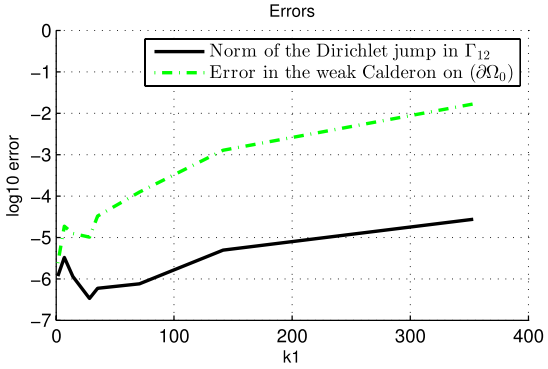

(a) Rule 3: $2N_i + 1 = 1.1 \max_i\{\kappa_i\} + 7$.

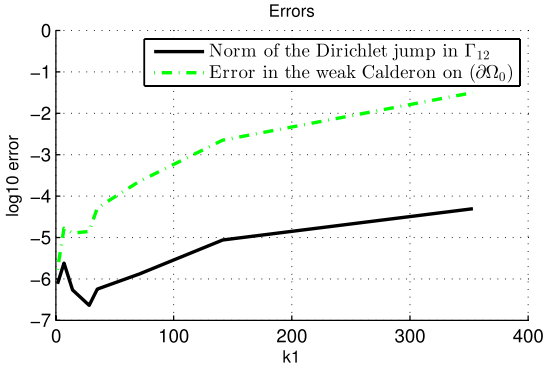

(b) Rule 3: $2N_i + 1 = 1.4 \max_i\{\kappa_i\} + 7$.

Fig. 7. Errors in different norms for increasing frequencies, $\kappa_0 \in [0, 250]$ asymmetric case.

4.5. Performance using iterative solvers—preconditioning

When the wavenumber increases, the Helmholtz equation becomes more indefinite, hence, the convergence rate of iterative solvers based on Krylov subspace, e.g. *Generalized Minimal Residual* (GMRes) method, is either poor or not achieved [31, Chapter 6]. To tackle this, one traditionally resorts to different preconditioning schemes [32–34].

The Calderón identity, used to establish MTF, leads to a built-in preconditioner given by the block diagonal operator,

$$\mathbf{A} := \begin{pmatrix} \mathsf{A}_0 & 0 & 0 \\ 0 & \mathsf{A}_1 & 0 \\ 0 & 0 & \mathsf{A}_2 \end{pmatrix}, \tag{60}$$

whose discrete form is already computed. More precisely, the discrete Calderón identity becomes a mass-like matrix M_{as} with a block diagonal composed by duality products. The duality pairings for the Neumann trace yield an identity-like matrix

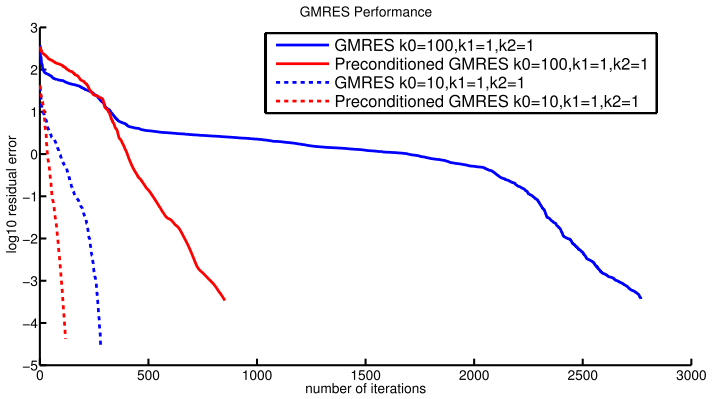

(a) Symmetric case: $\kappa_1 = \kappa_2 = 1$, Size: 420 ($\kappa_0 = 10$) and 3084 ($\kappa_0 = 100$).

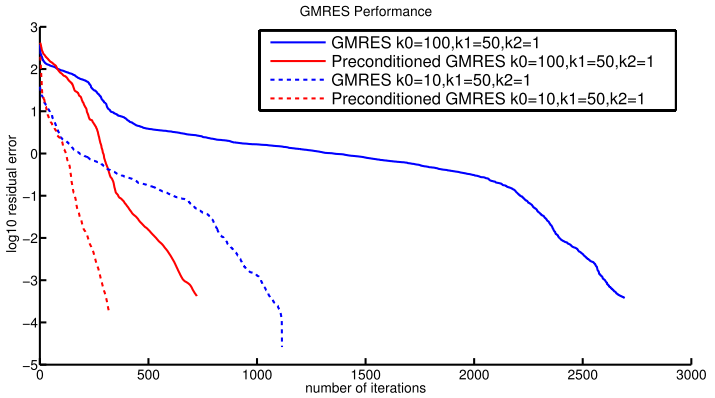

(b) Asymmetric case: $\kappa_1 = 50$, $\kappa_2 = 1$, Size: 1232 ($\kappa_0 = 10$) and 3084 ($\kappa_0 = 100$).

Fig. 8. Residual error in two-norm against number of iterations for GMRes (no restart). The preconditioner is applied on the left side of the linear system.

due to the orthogonality of first-kind Chebyshev polynomials, while for Dirichlet traces one obtains a bi-diagonal matrix coming from recursion and orthogonality properties between first and second kind Chebyshev polynomials.

The preconditioning matrix explicitly reads,

$$\mathsf{P} = \mathsf{M}_{ass}^{-1}\mathbf{A} \tag{61}$$

where $\mathbf{A}$ is the discretization of (60) and M_{ass}^{-1} is the mass-like matrix. Since the structure of the mass matrix is diagonal per block, the numerical cost of its inverted matrix–vector product is negligible compared to the dense matrix–vector product originated by $\mathbf{A}$. We use the naive strategy to carry out a LU-factorization of the relative small bi-diagonal blocks, which means a simple reordering, and then perform sparse substitutions at each iteration of GMres method.

Note that the discretization form used in (60) to build the preconditioner is not necessarily the optimal one to tackle the wavenumber dependency [35,36]. However, the proposed preconditioner requires a negligible numerical cost.

Fig. 8 shows the convergence history for a homogeneous case ($\kappa_1 = \kappa_2 = 1$) and a heterogeneous case ($\kappa_1 = 50$, $\kappa_2 = 1$), both comparing GMRes [37] without and with the block diagonal preconditioner proposed P, at moderate frequency ($\kappa_0 = 10$) and high frequency ($\kappa_0 = 100$). One can observe the significant reduction in number of iterations for the preconditioned system, while the convergence of the un-preconditioned system becomes unacceptable. In terms of CPU time, the solution by GMRes without preconditioner (resp. with), including preprocessing of factorization, requires 18 s (resp. 2 s) for the case $\kappa_0 = 10$, $\kappa_1 = 50 \mid 1$, $\kappa_2 = 1$, and 245 s (resp. 30 s) for the case $\kappa_0 = 100$, $\kappa_1 = 50 \mid 1$, $\kappa_2 = 1$.

5. Conclusions and future work

We have presented a robust and efficient method that allows the modeling of scattering by heterogeneous penetrable scatters for large frequency ranges. Robustness is due to the lack of spurious modes and large frequency sweep that can be practically handled. Efficiency comes from two sources: the parallelizable character of the formulation along with the choice of discretization bases. Computation of matrix entries resulting from the Galerkin–Petrov discretization proposed can be quickly computed using FFT and regularization techniques. Moreover, the method yields a built-in preconditioner, as its diagonal and mass matrix can be reused to improve convergence of iterative solvers as GMRes, just as previously

shown for low-order elements. Nonetheless, although a rule of thumb has been given to obtain the number of Chebyshev polynomials required, better estimates should be sought after. Also, particular attention should be given to integration routines for boundary integral operator.

Future research directions focus on a more detailed study of related preconditioning schemes: their dependency on wavenumbers, contrast and relation to operator preconditioning. Also, we intend to continue improving code efficiency by accelerating matrix–vectors computations by compression and its extension three-dimensions.

Acknowledgment

We thank Prof. Oscar Bruno for his valuable comments over a discussion concerning a draft of the present work.

References

[1] S.A. Sauter, C. Schwab, Boundary Element Methods, in: Springer Series in Computational Mathematics, vol. 39, Springer-Verlag, Berlin, 2011, http://dx.doi.org/10.1007/978-3-540-68093-2. translated and expanded from the 2004 German original. URL: http://dx.doi.org/10.1007/978-3-540-68093-2.
[2] E. Darve, P. Havé, Efficient fast multipole method for low-frequency scattering, J. Comput. Phys. 197 (1) (2004) 341–363. http://dx.doi.org/10.1016/j.jcp.2003.12.002. URL: http://dx.doi.org/10.1016/j.jcp.2003.12.002.
[3] E. Darve, P. Havé, A fast multipole method for Maxwell equations stable at all frequencies, Philos. Trans. R. Soc. Lond. Ser. A Math. Phys. Eng. Sci. 362 (1816) (2004) 603–628. http://dx.doi.org/10.1098/rsta.2003.1337. URL: http://dx.doi.org/10.1098/rsta.2003.1337.
[4] E. Darrigrand, Coupling of fast multipole method and microlocal discretization for the 3-D Helmholtz equation, J. Comput. Phys. 181 (1) (2002) 126–154. http://dx.doi.org/10.1006/jcph.2002.7091. URL: http://dx.doi.org/10.1006/jcph.2002.7091.
[5] J.T. Chen, Y.P. Chiu, On the pseudo-differential operators in the dual boundary integral equations using degenerate kernels and circulants, Eng. Anal. Bound. Elem. 26 (1) (2002) 41–53.
[6] P.D. Lin, New Computation Methods for Geometrical Optics, in: Springer Series in Optical Sciences, vol. 178, Springer, Singapore, 2014, http://dx.doi.org/10.1007/978-981-4451-79-6. URL: http://dx.doi.org/10.1007/978-981-4451-79-6.
[7] T.G. Philbin, Making geometrical optics exact, J. Modern Opt. 61 (7) (2014) 552–557. http://dx.doi.org/10.1080/09500340.2014.899646. URL: http://dx.doi.org/10.1080/09500340.2014.899646.
[8] O.P. Bruno, F. Reitich, High-order methods for high-frequency scattering applications, in: Modeling and Computations in Electromagnetics, in: Lect. Notes Comput. Sci. Eng., vol. 59, Springer, Berlin, 2008, pp. 129–163. http://dx.doi.org/10.1007/978-3-540-73778-0_5. URL: http://dx.doi.org/10.1007/978-3-540-73778-0_5.
[9] O.P. Bruno, S.K. Lintner, A high-order integral solver for scalar problems of diffraction by screens and apertures in three-dimensional space, J. Comput. Phys. 252 (2013) 250–274. http://dx.doi.org/10.1016/j.jcp.2013.06.022. URL: http://dx.doi.org/10.1016/j.jcp.2013.06.022.
[10] A. de La Bourdonnaye, High frequency approximation of integral equations modeling scattering phenomena, RAIRO Modél. Math. Anal. Numér. 28 (2) (1994) 223–241.
[11] S.N. Chandler-Wilde, I.G. Graham, S. Langdon, E.A. Spence, Numerical-asymptotic boundary integral methods in high-frequency acoustic scattering, Acta Numer. 21 (2012) 89–305.
[12] D.P. Hewett, S. Langdon, J.M. Melenk, A high frequency *hp* boundary element method for scattering by convex polygons, SIAM J. Numer. Anal. 51 (1) (2013) 629–653. http://dx.doi.org/10.1137/110856812. URL: http://dx.doi.org/10.1137/110856812.
[13] V. Domínguez, I.G. Graham, V.P. Smyshlyaev, A hybrid numerical-asymptotic boundary integral method for high-frequency acoustic scattering, Numer. Math. 106 (3) (2007) 471–510. http://dx.doi.org/10.1007/s00211-007-0071-4. URL: http://dx.doi.org/10.1007/s00211-007-0071-4.
[14] F. Ecevit, F. Reitich, Analysis of multiple scattering iterations for high-frequency scattering problems. I. The two-dimensional case, Numer. Math. 114 (2) (2009) 271–354. http://dx.doi.org/10.1007/s00211-009-0249-z. URL: http://dx.doi.org/10.1007/s00211-009-0249-z.
[15] A. Anand, Y. Boubendir, F. Ecevit, F. Reitich, Analysis of multiple scattering iterations for high-frequency scattering problems. II. The three-dimensional scalar case, Numer. Math. 114 (3) (2010) 373–427. http://dx.doi.org/10.1007/s00211-009-0263-1. URL: http://dx.doi.org/10.1007/s00211-009-0263-1.
[16] S.L. Samuel, P. Groth, David P. Hewett, Hybrid numerical-asymptotic approximation for high frequency scattering by penetrable convex polygons, Preprint MPS-2013-02, Department of Mathematics and Statistics, University of Reading, 2013.
[17] R. Hiptmair, C. Jerez-Hanckes, Multiple traces boundary integral formulation for Helmholtz transmission problems, Adv. Comput. Math. 37 (1) (2012) 39–91. http://dx.doi.org/10.1007/s10444-011-9194-3. URL: http://link.springer.com/10.1007/s10444-011-9194-3.
[18] X. Claeys, R. Hiptmair, C. Jerez-Hanckes, Multitrace boundary integral equations, in: Direct and Inverse Problems in Wave Propagation and Applications, in: Radon Ser. Comput. Appl. Math., vol. 14, De Gruyter, Berlin, 2013, pp. 51–100.
[19] X. Claeys, R. Hiptmair, Multi-trace boundary integral formulation for acoustic scattering by composite structures, Comm. Pure Appl. Math. 66 (8) (2013) 1163–1201. http://dx.doi.org/10.1002/cpa.21462. URL: http://dx.doi.org/10.1002/cpa.21462.
[20] X. Claeys, R. Hiptmair, C. Jerez-Hanckes, S. Pintarelli, Novel multi-trace boundary integral equations for transmission boundary value problems, Tech. Rep. 2014-5, Seminar for Applied Mathematics, ETH Zurich, 2014, February.
[21] W. McLean, Strongly Elliptic Systems and Boundary Integral Equations, Cambridge University Press, Cambridge, 2000.
[22] M. Abramowitz, Handbook of Mathematical Functions with Formulas, Graphs, and Mathematical Tables, 1988, http://dx.doi.org/10.1119/1.15378.
[23] C. Jerez-Hanckes, J.-C. Nédélec, Explicit variational forms for the inverses of integral logarithmic operators over an interval, SIAM J. Math. Anal. 44 (4) (2012) 2666–2694. http://dx.doi.org/10.1137/100806771. URL: http://dx.doi.org/10.1137/100806771.
[24] J.-L. Lions, E. Magenes, Problèmes aux Limites Non Homogènes et Applications. Vol. 1, in: Travaux et Recherches Mathématiques, No. 17, Dunod, Paris, 1968.
[25] P. Grisvard, Elliptic Problems in Nonsmooth Domains, in: Monographs and Studies in Mathematics, vol. 24, Pitman (Advanced Publishing Program), Boston, MA, 1985.
[26] L.N. Trefethen, Approximation Theory and Approximation Practice, Society for Industrial and Applied Mathematics (SIAM), Philadelphia, PA, 2013.
[27] F.Q. Hu, A spectral boundary integral equation method for the 2-D Helmholtz equation, Comput. Phys. 120 (2) (1995) 340–347.
[28] R. Hiptmair, C. Jerez-Hanckes, C. Urzúa-Torres, Mesh-independent operator preconditioning for boundary elements on open curves, SIAM J. Numer. Anal. 52 (5) (2014) 2295–2314.
[29] O. Steinbach, Numerical Approximation Methods for Elliptic Boundary Value Problems: Finite and Boundary Elements, Springer, New York, 2008, http://dx.doi.org/10.1007/978-0-387-68805-3. URL: http://dx.doi.org/10.1007/978-0-387-68805-3. Translated from German (2003).
[30] K. Warnick, Numerical Analysis for Electromagnetic Integral Equations, Artech House, Norwood, MA, 2008.
[31] Y. Saad, Iterative Methods for Sparse Linear Systems, second ed., Society for Industrial Mathematics, 2002.
[32] O. Ernst, M. Gander, Why it is difficult to solve Helmholtz problems with classical iterative methods, in: Numerical Analysis of Multiscale Problems, Springer, 2012, pp. 325–363.
[33] Y. Erlangga, Advances in iterative methods and preconditioners for the Helmholtz equation, Arch. Comput. Methods Eng. 15 (2008) 37–66. http://dx.doi.org/10.1007/s11831-007-9013-7. URL: http://dx.doi.org/10.1007/s11831-007-9013-7.

[34] M. Benzi, Preconditioning techniques for large linear systems: a survey, J. Comput. Phys. 182 (2002) 418–477. http://dx.doi.org/10.1006/jcph.2002.7176.
[35] R. Hiptmair, Operator preconditioning, Comput. Math. Appl. 52 (5) (2006) 699–706. http://dx.doi.org/10.1016/j.camwa.2006.10.008. URL: http://www.sciencedirect.com/science/article/pii/S0898122106002495.
[36] O. Steinbach, W. Wendland, The construction of some efficient preconditioners in the boundary element method, Adv. Comput. Math. 9 (1998) 191–216. http://dx.doi.org/10.1023/A:1018937506719.
[37] Y. Saad, M.H. Schultz, GMRes: a generalized minimal residual algorithm for solving non symetric linear systems, SIAM J. Stat. Comput. 7 (3) (1986).